JBUON 2020; 25(2): 1237-1244
ISSN: 1107-0625, online ISSN: 2241-6293 • www.jbuon.com
Email: editorial_office@jbuon.com

ORIGINAL ARTICLE

The utility of texture-based classification of different types of ascites on magnetic resonance

Paul-Andrei Stefan[1,2], Marius-Emil Puscas[3,4], Csaba Csuak[2,5], Andrei Lebovici[2,5], Bianca Petresc[2], Roxana Lupean[6,7], Carmen Mihaela Mihu[2,6]

[1]Anatomy and Embryology, Morphological Sciences Department, "Iuliu Hatieganu" University of Medicine and Pharmacy, Cluj-Napoca. [2]Radiology and Imaging Department, County Emergency Hospital, Cluj-Napoca. [3]Oncological Surgery and Gynecologic Oncology, Surgery Department, "Iuliu Hatieganu" University of Medicine and Pharmacy, Cluj-Napoca. [4]General Surgery Department, Institute of Oncology "Prof.Dr. Ion Chiricuta", Cluj-Napoca. [5]Radiology Department, "Iuliu Hatieganu" University of Medicine and Pharmacy, Cluj-Napoca. [6]Histology, Morphological Sciences Department, "Iuliu Hatieganu" University of Medicine and Pharmacy, Cluj-Napoca. [7]Obstetrics and Gynecology Clinic "Dominic Stanca", County Emergency Hospital, Cluj-Napoca, Romania

Summary

Purpose: *To quantify the texture characteristics of different types of ascitic fluid on magnetic resonance (MR) images and to determine their utility for computer-assisted lesion classification.*

Methods: *The MR images of 48 patients with intra-abdominal collections were retrospectively analyzed. Patients were grouped according to the underlying disease and pathological outcomes. The fluid texture was analyzed on a breath hold T2-weighted sequence, using MaZda software. Most discriminative texture features for the classification of different types of ascites were selected based on Fisher coefficients (F) and the probability of classification error and average correlation coefficients (POE+ACC). Computer-assisted classification based on k-nearest-neighbor (k-NN) and artificial neural networks (ANN) was performed and accuracy, sensitivity and specificity were calculated.*

Results: *Adequate discriminative power for differentiating benign from malignant ascites was achieved for two textural features, namely the Run Length Nonuniformity computed from both vertical and horizontal directions with 91.84% accuracy (sensitivity 100%; specificity 42.86%), and ten features for differentiating bland from hemorrhagic fluid with 90% accuracy (sensitivity 92.31%; specificity 85.71%), both for the ANN classifier.*

Conclusion: *Texture analysis revealed several differences in signal characteristics of benign and malignant ascites. Computer-assisted pattern recognition algorithms may improve the diagnosis of ascites, especially in the early stages when there are few peritoneal modifications or when the cause is difficult to find.*

Key words: *ascites, diagnostic aid, image processing, magnetic resonance, texture-based analysis*

Introduction

Ascites represents an abnormal fluid accumulation in the peritoneal cavity, which can occur due to local or systemic causes [1]. While ultrasonography (US) is considered to be the gold standard for the detection of ascites [2] and can be useful to characterize its content [3], magnetic resonance imaging (MRI) is usually reserved for selected cases. Nevertheless, MRI can offer a more accurate characterization of fluid collections based on their composition [4].

From a practical point of view, radiologists rarely have the purpose to elaborately analyze the

Corresponding author: Marius Emil Puscas, PhD. Oncological Surgery and Gynecologic Oncology, Surgery Department, "Iuliu Hatieganu" University of Medicine and Pharmacy, Cluj-Napoca and General Surgery Department, Institute of Oncology "Prof. Dr. Ion Chiricuta", Cluj-Napoca, Romania. Republicii Street, no. 34-36, 400015, Cluj-Napoca, Romania.
Tel: +40 746051833, Email: mariusemilpuscas@gmail.com
Received: 24/07/2019; Accepted: 01/11/2019

characteristics of the ascitic fluid, mostly focusing on investigating the leading pathology. However, the composition and physical properties of the liquid may vary, depending on the underlying disease and can be characteristic for a certain pathological process [5]. Although small differences among the types of ascites (at a cytological and biochemical level) rarely produce visible changes in the MRI signal, the diagnostic information exists in the texture of the image and can be quantified [6].

Texture analysis (TA) is a field of ongoing research, based on the extraction and processing of image-specific parameters. By quantifying the distribution patterns and intensity of the pixels in an image, TA aims to create an objective description of the image content [7]. In recent years, this technique has been integrated into computer-aided diagnosis [8].

In the present study, texture analysis was used for quantification of image features of the ascitic fluid on MRI examinations. The aim was to determine whether differences in signal characteristics exist among different origin types of intra-peritoneal collections and could be used for computer-assisted discrimination.

Methods

This Health Insurance Portability and Accountability Act–compliant, single-institution, pilot-study has been approved by the institutional review board and a waiver of informed consent was obtained due to its retrospective nature. In a radiological database, abdominopelvic MRI reports were searched from September 2016 to March 2019 by using the keyword "ascites". The original search yielded 512 reports. Each report was then analyzed and those studies in which the keyword in the report did not refer to the presence of ascites were excluded. The remaining 208 studies were reviewed by a radiologist blinded to the patient's clinical picture. Other exclusion criteria were as follows: the presence of a small amount of ascitic fluid(n=67), the presence of artifacts within the fluid (n=42), individuals with undocumented underlying disease (n=17), and patients with simultaneous pathologies that might have caused ascites (n=34). Finally, 48 patients were included in the study (22 females and 26 males; mean age 65.08 years, range 46-87 years).

Firstly, the patients were divided into 5 groups according to the pathology that causes ascites as follows: *group-A* (n=14): cirrhosis without imaging evidence of hepatocellular carcinoma (HCC); *group-B* (n=15): HCC associated with cirrhosis; *group-C* (n=7): peritoneal car-

Table 1. Main groups based on ascites-causing pathology and number of subjects with each disease

Main group	*Underlying pathology*	*Number of subjects*
Group A - cirrhosis without imaging evidence of hepatocellular carcinoma (n=14)	virus B-related cirrhosis	1
	virus C-related cirrhosis	4
	alcoholic cirrhosis	6
	Primary biliary cirrhosis	1
	autoimmune cirrhosis	1
	alcoholic cirrhosis synchronous with the infection with B virus	1
Group B - hepatocellular carcinoma associated with cirrhosis (n=15)	virus B-related cirrhosis	3
	virus C-related cirrhosis	4
	alcoholic cirrhosis	8
Group C- peritoneal carcinomatosis (n=7)	endometrial carcinoma	2
	high grade serous ovarian carcinoma	1
	serous peritoneal carcinoma	1
	prostatic adenocarcinoma	1
	pancreas adenocarcinoma	1
	renal cell carcinoma	1
Group D - secondary peritonitis and other intra-abdominal collections (n=5)	peritoneal tuberculosis	1
	subphrenic abscess	1
	uroperitoneum	1
	bile peritonitis	1
	necrosis of the intestinal wall	1
Group E - pancreatitis-related collections (n=7)	pancreatic ascites	2
	acute peri-pancreatic fluid collections	2
	pseudocysts	1
	infected fluid collections	2

cinomatosis (PC); *group-D* (n=5): secondary peritonitis and other intra-abdominal collections, and *group-E* (n=7); pancreatitis-related collections (Table 1).

Secondly, from the main 5 groups, patients were extracted for six other subgroups based on the characteristics of the ascitic fluid in order to be compared two by two: *group-F* (n=29): transudate vs. *group-G* (n=15); exudate, *group-H* (n=14): bland fluid vs. *group-I* (n=4): hemorrhagic fluid, *group-J* (n=27): benign fluid vs. *group-K* (n=7): malignant fluid. Subjects from the same main group were included in more than one subgroup, but subgroups containing the same individuals were not compared to each other (Table 2).

Reference standard

None of the patients with cirrhosis without imaging evidence of HCC underwent liver puncture for the diagnosis of the hepatic disease. Nine cases of ascites in this group were evaluated by paracentesis, three of which were assessed by MRI examinations before and after the puncture.

Among the subjects with HCC associated with cirrhosis, none of them had imaging evidence of peritoneal changes at the time of examination. The diagnosis of HCC had been confirmed by liver puncture in six patients, while the diagnosis was made by imaging, clinical, and laboratory findings in other patients. Six cases of ascites were evaluated by paracentesis, two of which underwent MRI examinations before and after the puncture. Because their cytology was benign, they were also included in group-J.

At the time of the examinations, all the subjects from the PC group were experiencing peritoneal changes visible on MR. Ascites was investigated by fluid aspiration (in four cases) or surgical biopsy (in three cases), with cytological confirmation of malignancy. Presence of ascites in the greater and lesser sac was found in one patient, two patients had gallbladder wall thickening, and the omental cake sign was not encountered in any individual. Besides ascites, peritoneal implants were the only modification found in the peritoneum in four patients.

All the subjects with secondary peritonitis and other intra-abdominal collections underwent surgery for the underlying condition and ascites fluid analysis was performed from the surgical sampling. One individual diag-

Table 2. Distribution of patients into secondary groups

Secondary group	*Subjects from the main groups*	*Total number of patients*
group F- transudate	Group A - 14	29
	Group B - 15	
group G-exudate	Group C - 5	15
	Group D - 5	
	Group E - 5	
group H-bland fluid	Group A - 7	14
	Group B - 5	
	Group C - 1	
	Group E - 1	
group I- hemorrhagic fluid	Group C - 4	4
group J-benign fluid	Group A - 9	27
	Group B - 6	
	Group D - 5	
	Group E - 7	
group K-malignant fluid	Group C - 7	7

Table 3. The ratio of pathologically confirmed cases and the time elapsed (measured in days) from the MR examination to the pathological analysis

Group	*Pathologically confirmed cases (number/total)*	*Time elapsed (days: mean + range)*	
		Before MR	*After MR*
A	9/14	122.8 (50-191)	74.8 (58-124)
B	6/15	212.3 (192-256)	143.6 (142-156)
C	7/7	52 (36-68)	46.3 (30-78)
D	5/5	2	8.2 (1-27)
E	4/7	12	15.4 (13-28)

MR: Magnetic resonance imaging

nosed with peritoneal tuberculosis underwent surgical biopsy of the peritoneum, which confirmed the presence of inflammatory granulomatous necrosis. One patient had a perinephric abscess with anterior extention, which led to a sub-phrenic collection. Two patients developed iatrogenic intra-abdominal collection; the first one was due to bladder perforation secondary to percutaneous suprapubic catheterization and the second one occurred after laparoscopic cholecystectomy. One subject had secondary peritonitis following intestinal wall necrosis .

Non-surgical behavior was applied to the subjects with acute peri-pancreatic fluid collections and their resolution was noted at subsequent ultrasound examinations (41 and 59 days, respectively) after the acute episode. Surgery was performed in case of infected collections and pancreatic pseudocyst and one individual with ascites underwent fluid aspiration. The number of pathologically confirmed cases from each group as well as the time elapsed (measured in days) from the MR examination to the pathological analysis of the fluid are shown in Table 3.

MRI protocol

All scans were performed on the same unit (1.5-T, SIGNA™ Explorer, General Electric) using a multi-coil phased array. No routine anti-peristaltic drugs were used; however, a narrow band around the abdomen was applied to diminish the intestinal peristalsis. The acquisition protocol consisted of Axial T1 In and Out-of-phase, Axial T2 periodically rotated overlapping parallel lines with enhanced reconstruction (propeller), breath hold axial t2 Fat saturated (FatSat) fast imaging employing steady-state acquisition (FIESTA) Axial diffusion-weighted imaging (DWI), and contrast-enhanced T1-weighted fat-suppressed. The imaging protocol varied because the examinations were selected from a range of three years, but each MRI examination comprised a Breath Hold Axial T2 FatSat FIESTA (repetition time ms/echo time ms, 5.1/2.3; inversion time, 200 ms; section thickness, 4 mm; slice spacing, 0.4 mm; bandwidth, 62.5 Hz/pixel; field of view, 44x39.6; matrix, 256x320; NEX, 1; slices, 44), which was the only sequence evaluated in this study.

Texture analysis and fluid classification

Each examination was reviewed individually on the Breath Hold Axial T2 FatSat FIESTA sequence and the slice containing the most eloquent characteristics of the ascites fluid was selected. Representative slices were saved in DICOM format (Digital Imaging and Communications in Medicine) and imported into a free-available textural analysis software, MaZda version 5 [9] (URL: https://data.mendeley.com/datasets/dkxyrzwpzs/).

In order to diminish the influence of contrast and brightness variations which could affect the true texture of the image, gray-level normalization for each region of interest (ROI) was conducted by using the limitation of dynamics to $\mu \pm 3\sigma$ (μ=gray-level mean; and σ=gray-level standard deviation) [10]. For the definition and positioning of ROIs, MaZda 5 provides a semi-automatic level-set technique that does not require manual delineation of the structure of interest contours, thus not being necessary to assess the inter- or intra-observer reproducibility in the current study (Figure 1). For each ROI, texture features derived from the gray-level histogram, co-occurrence matrix, run-length matrix, and the absolute gradient were calculated (for details: http://www.eletel.p.lodz.pl/mazda/download/mazda_manual.pdf).

Two sets (each containing 10 texture features that were optimized for differentiating between ascites categories) were selected using two methods. Firstly, based on Fisher coefficients (F, the ratio of between-class to within-class variance), which selects features that have high discriminatory power and are also well-correlated with each other. Secondly, based on POE+ACC (P, a combined measure of the probability of classification error and correlation between features), providing features that are best suited for classification [6]. Selected parameters provided by these methods were imported into the B11 program (part of MaZda package) for further processing of the data. In order to distinguish between different groups and subgroups, two nonlinear supervised classifiers were used: the k-nearest-neighbor (k-NN) classifier (which follows partitioning method for clustering) [11] and Artificial Neural NetworkS (ANN) which simulates the way a human brain processes information by separating clusters belonging to different classes [6].

Statistics

In order to differentiate between features with poor and good discriminatory potential, an F>2 value for Fisher coefficients was used as a cut-off. Accuracy, sensitivity and specificity were calculated separately for each parameter selection test and classification method, in order to measure the practical value of the extracted textural information. Statistical analyses were performed using a commercially-available dedicated software MedCalc, version 9.2.0.0 (MedCalc Software, Mariakerke, Belgium).

Results

Selected Fisher coefficients were derived mostly from first and second-order texture features and from the co-occurrence matrix (Table 4). The ANN classifier generally provided higher rates of correct classification than did the k-NN classifier (Table 5).

When comparing group A to B, the results showed that one patient with cirrhosis and two with HCC were misclassified by both k-NN and ANN. The same practical value (expressed by accuracy and specificity) was obtained by ANN for both parameters selection methods. Fisher coefficients were low (F<1) for all parameters, with entropy being the dominant parameter following both selection methods.

With regard to the differentiation of benign ascites from malignant ascites (group J versus K), the ANN classifier provided better rates of correct classification than did k-NN, with the most accu-

Table 4. Ranking of the best 10 texture features for group differentiation, based on Fisher and POE + ACC coefficients

Group A versus B		*Group J versus K*	
Fisher	*POE+ACC*	*Fisher*	*POE+ACC*
CZ2S6Entropy (F=0.76)	CZ2S6Entropy (P=0.38)	RVS6RLNonUni (F=2.29)	CN2S6SumAverg (P=0.3)
CH5S6InvDfMom (F=0.69)	CN3S6SumOfSqs (P=0.41)	RHS6RLNonUni (F=2.05)	WavEnHL_s-4 (P=0.31)
CZ3S6Entropy (F=0.69)	CN5S6Contrast (P=0.45)	RZS6RLNonUni (F=1.99)	CH5S6SumAverg (P=0.33)
CZ4S6Entropy (F=0.67)	RHS6RLNonUni (P=0.48)	RNS6RLNonUni (F=1.70)	CN5S6AngScMom (P=0.34)
CZ5S6AngScMom(F=0.63)	CZ3S6AngScMom (P=0.48)	RVS6GLevNonU (F=1.3)	CN5S6InvDfMom (P=0.35)
CH2S6Entropy (F=0.63)	WavEnLH_s-4 (P=0.49)	RHS6GLevNonU(F=1.23)	CN1S6SumAverg (P=0.39)
CH4S6InvDfMom (F=0.63)	CZ5S6SumOfSqs (P=0.49)	RZS6GLevNonU(F=1.12)	CH4S6SumAverg (P=0.4)
CZ5S6Entropy (F=0.62)	CH1S6SumOfSqs (P=0.50)	RNS6GLevNonU(F=1.04)	CZ5S6SumOfSqs (P=0.4)
CN2S6Entropy(F=0.62)	CN5S6InvDfMom (P=0.51)	CN2S6Entropy(F=0.85)	Variance (P=0.4)
CV5S6Entropy(F=0.61)	CH5S6SumVarnc (P=0.68)	CV4S6Entropy (F=0.82)	CN5S6DifVarnc (P=0.51)
Group H versus I		*Group F versus G*	
Fisher	*POE+ACC*	*Fisher*	*POE+ACC*
Perc90 (F=5)	Mean (P=0.15)	CZ1S6Contrast (F=1.06)	CV4S6DifEntrp (P=0.38)
Mean (F=4.17)	CN2S6AngScMom (P=0.23)	WavEnLL_s-1 (F=1.05)	CV5S6SumAverg (P=0.41)
Perc50 (F=4.)	WavEnLH_s-2(P=0.26)	CZ1S6Correlat (F=1.02)	CZ4S6AngScMom (P=0.44)
Perc99 (F=4.)	CN2S6Entropy (P=0.29)	CV3S6Contrast (F=1.01)	Perc10 (P=0.45)
CN2S6Entropy (F=4.04)	Perc50 (P=0.29)	CV3S6Correlat (F=1)	CV3S6Correlat (P=0.46)
CN3S6Entropy (F=3.68)	CN4S6Contrast (P=0.32)	WavEnHL_s-4 (F=0.99)	CV3S6SumOfSqs (P=0.47)
RVS6RLNonUni (F=2.95)	CN3S6AngScMom (P=0.33)	CZ2S6Contrast (F=0.98)	CH1S6SumAverg (P=0.47)
CN1S6Entropy (F=2.88)	CV3S6Entropy (P=0.35)	CZ2S6Correlat (F=0.98)	Variance (P=0.48)
CV3S6Entropy (F=2.84)	CN5S6DifVarnc (P=0.35)	CV2S6Correlat (F=0.94)	CN3S6AngScMom (P=0.49)
CV2S6Entropy (F=2.72)	WavEnHL_s-4 (P=0.36)	CV2S6SumVarnc (F=0.93)	WavEnHL_s-4 (P=0.58)

Entropy (entropy), InvDfMom (inverse difference moment), AngScMom (angular second moment), SumOfSqs (sum of squares), Contrast (contrast), RLNonUni (run length nonuniformity), WavEn (wavelet energy),SumVarnc (sum variance), GLevNonU (grey level nonuniformity), SumAverg (sum average), Variance (histogram's variance), DifVarnc (difference variance), Perc.90% (90% percentile), Mean (histogram's mean), Perc.50% (50% percentile), Perc.99% (99% percentile), Perc.10% (10% percentile), DifEntrp (difference entropy), Correlat (correlation)

Table 5. Results of k-NN and ANN classification of ascites fluids, using texture features extracted by the Fisher and the POE+ACC method; all the values are expressed as percentages

Compared groups	*Method of selection*	*Method of classification*	*Accuracy*	*Sensitivity*	*Specificity*
Group A and B	Fisher	k-NN	41.38	42.86	40
		ANN	89.66	92.86	86.67
	POE+ACC	k-NN	55.17	57.14	53.33
		ANN	89.66	92.86	86.67
Group C and J	Fisher	k-NN	77.55	85.71	28.57
		ANN	91.84	100	42.86
	POE+ACC	k-NN	79.59	90.48	14.29
		ANN	85.71	100	0.00
Group H and I	Fisher	k-NN	76.47	84.62	50
		ANN	88.89	85.71	100
	POE+ACC	k-NN	60	61.54	57.14
		ANN	90	92.31	85.71
Group F and G	Fisher	k-NN	63.04	65.52	58.82
		ANN	86.96	86.21	88.24
	POE+ACC	k-NN	50	58.62	35.29
		ANN	93.48	96.55	88.24

POE+ACC: Probability of classification error and average correlation coefficients), K-NN: K-Nearest-Neighbor), ANN: artificial neural networks

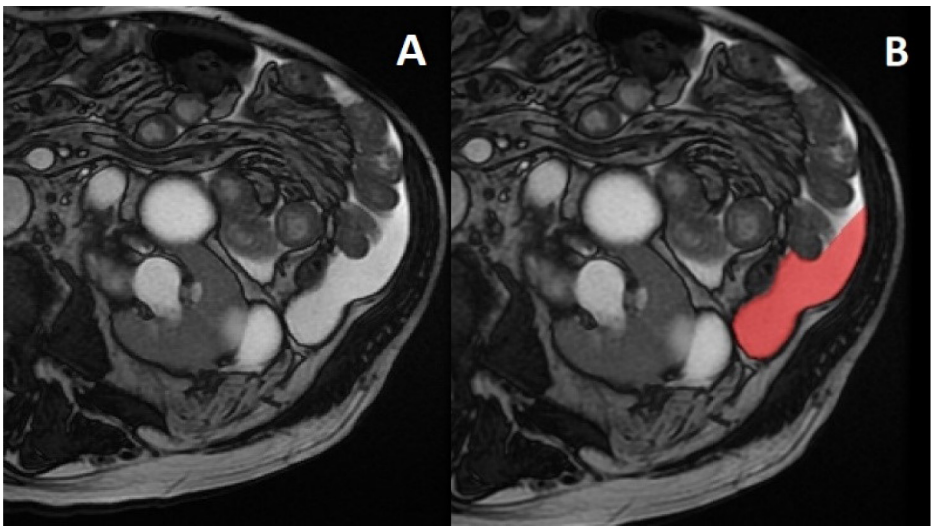

Figure 1. A: Breath Hold Axial T2 FatSat FIESTA MR image of an 87-year-old with histologically proven peritoneal tuberculosis. **B:** The slice with the region of interest (red area) used for textural analysis.

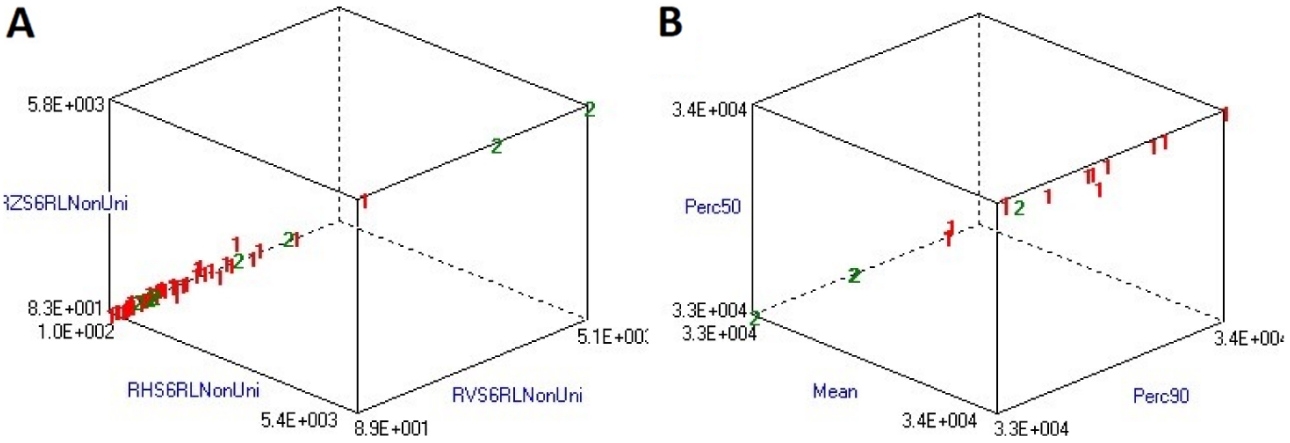

Figure 2. Three-dimensional illustrations of the distribution of vectors in the data space based on the three most discriminative texture features. **A:** benign ascites (red/1), malignant ascites (green/2); **B:** bland fluid (red/1), hemorrhagic fluid (green/2). RLNonUni: run length nonuniformity, Perc.50%: 50% percentile, Mean: histogram's mean, Perc.90%: 90% percentile

rate one being based on Fisher coefficients (accuracy 91.84%; sensitivity 100%, specificity 42.86%). A value of F>2 was achieved by two parameters, namely the Run Length Nonuniformity (RLNonUni) computed from both vertical and horizontal directions (Figure 2). The RLNonUni had lower values in benign ascites compared to malignant ascites for both directions. The average values of vertical and horizontal directions measured from benign ascites vs. malignant ascites were 727.51 and 834.78 vs. 1985.26 and 2127.78.

Analysis based on liquid appearance (bland vs hemorrhagic, group H vs I) held the highest F coefficients, with the parameters selected mainly from the first and second-order features provided by both selection methods. Mean was the dominant parameter by POE+ACC selection and second dominant by Fisher selection, with average values of 33621.5 for bland fluid and 33384.6 for the hemorrhagic liquid group. The best practical value was obtained by POE+ACC selected features using ANN classification (accuracy 90%; sensitivity 92.31%, specificity 85.71.%) (Figure 2).

Distinguishing transudate from exudate, two patients with carcinomatosis were classified by both k-NN and ANN as having transudate. The best practical value was obtained by POE+ACC selected features using ANN classification. Fisher coefficients were low (F<2) for all parameters.

Discussion

There is lack of studies that attempt to differentiate several categories of ascites based on MRI. This may be due to the fact that fluid often suffers from intense artifacts, mostly due to the patients'

respiratory movements. Considering this, a Breath Hold type sequence was chosen, which cancels the fat signal at the same time to better highlight the fluid content. MR was chosen as the examination method for the current study, mostly because it offers heterogeneous visual images [12], which could possibly provide an increased utility in characterizing different types of fluid contents.

Computer-aided diagnosis (CAD) has become one of the biggest subjects of interest in radiology. In recent years, it has evolved from a simple research topic to near implementation in clinical practice [13]. Texture analysis is a core component of CAD which, together with automated decision-making, promises major changes in the way radiologists interpret studies [14].

Some of the best results in the current study were obtained in the differentiation between benign and malignant ascites. Similar studies with the same objective mainly focus on the peritoneal changes and the overall assessment of intra-abdominal organs, but not on the actual analysis of the ascitic fluid. For ultrasonography, the sensitivity ranged from 38.10 to 80.95% in a study conducted by Khaladkar et al [3] and the accuracy reached to 93.5% in another research [1]; however, in both studies, results were admissible only after the inclusion of overall assessment of abdominal organs and the clinical data. The first study [3] also evaluates the discriminative power of computer tomography (CT), with a sensitivity of 57.14-80.95% and a specificity of 57.38-91.80%. Overall, the best results from these studies were obtained following the quantification of advanced changes of peritoneal carcinomatosis (greater and lesser sac ascites, omental cake, etc.). Only by the presence of peritoneal implants, the sensitivity decreased to 47.62% for US and 57.14% for CT, with 0% specificity in both cases. This was not the case in the current study, the omental cake sign was not encountered in any patient, and the presence of ascites in the greater and lesser sac was found only in one patient, suggesting that textural analysis can differentiate between benign and malignant ascites in the absence of advanced peritoneal changes, assessment of abdominal organs, or clinical data.

The run-length method quantifies pixels for certain directions , which have identical image value. The Run Length Nonuniformity increases when extreme values of gray levels dominate the histogram [15]. Thus, the fact that malignant ascites had higher RLNonUni values for both scan directions may reflect a more anarchic or heterogeneous aspect of the liquid (possibly due to higher or atypical cellularity), compared to the relative uniformity of the benign fluid.

Our results showed that computer-assisted classification failed to accurately differentiate between ascites of patients with cirrhosis and those with HCC. This is supported by both the pathological outcome of the fluid analysis (with no significant cytological differences between patients from group A and B who underwent fluid aspiration) and previous literature data reporting that HCC rarely metastasizes to the peritoneum, with cytology being almost never positive [16].

Regarding the difference between bland and hemorrhagic fluid (group H and group I), two of the cases pathologically described "hemorrhagic" were misclassified as "bland". The fluid provided from the same subjects was described at the pathological examination as being "slightly hemorrhagic", as opposed to the rest of the patients in group I who had a liquid with "hemorrhagic background". Therefore, it can be concluded that the two cases had lower blood content. The fact that the mean parameter had one of the best coefficients indicates that the average pixel intensity was significantly different between groups H and I, with higher values in the bland group than in the hemorrhagic one. This is most probably due to the fact that the blood dispersed in the ascites fluid decreased the MR signal intensity.

Unfortunately, in our center, the ascitic fluid analysis was limited to cytological examination in most cases. From this point of view, the patients' division in the transudate and exudate groups was a strictly theoretical one, based on what the literature data refer to as being the most frequent [5] and not the serum-ascites albumin gradient, hence providing the poor results.

A similar study was conducted by Baroud et al [17], who analyzed the textural features of the ascites fluid on CT examinations, with a different method for data selection (Fisher and Mutual Information) and a different model (linear discriminant analysis) to classify the data. The results obtained were similar to the present study (the accuracy of the differentiation of the malignant fluid from the benign fluid was 86.5%), which may indicate that the textural analysis of the ascites can be successfully applied on both CT and MR examinations and can prove to be useful.

From our knowledge, no study involving textural analysis of a fluid content on MRI has been carried out so far. An advantage of this study is that all the images were extracted from the same examination protocol, the same sequence, and the same machine, providing a higher degree of homogeneity of images.

Because the study included a limited group of patients, it could not be divided into training

and validation sets within the ANN classifier. For future implementation, the ANN classifier must be trained on a larger number of images in order to be able to correctly classify the ones to which it has not been exposed [6]. In addition, another limitation of this study is the fact that selected examinations did not include all possible causes of intra-peritoneal collections (appendicitis, perforated ulcers, etc.), as well as the fact that some of the patients were not subjected to ascites fluid pathological examination for various reasons.

In conclusion, computer-assisted discrimination between different types of ascitic fluid showed important textural differences between benign and malignant groups and bland-hemorrhagic groups. If confirmed by larger batches of patients, computer-assisted diagnosis could be really useful in current practice, guiding practitioners towards a possible cause of ascites that is difficult to highlight, especially in the presence of few peritoneal modifications or small quantity of fluid.

Ethics

This article was approved by the local ethics committee and is in accordance with the Helsinki Declaration.

Conflict of interests

The authors declare no conflict of interests.

References

1. Smereczyński A, Katarzyna K, Elżbieta Bernatowicz E. Difficulties in differentiating the nature of ascites based on ultrasound imaging. J Ultrason 2007;17:96-100.
2. Fagan MJ. Cirrhosis. In: Alguire PC, American College of Physicians, Clerkship Directors in Internal Medicine in: Internal Medicine Essentials for Clerkship Students (2nd Edn). ACP Press; 2009, pp 83-6.
3. Khaladkar SM, Gujarath A, Thakkar D et al. Differentiation of malignant and benign ascites by Ultrasonography and/or CT. Int J Healthcare Biomed Res 2015;3:102-16.
4. Mansoori B, Herrmann KA. Mesentery, Omentum. Peritoneum: Fluid Collections (Ascites, Abscess, Hemorrhage). In: Hamm B, Ros PR. Abdominal Imaging. Berlin, Heidelberg: Springer Berlin Heidelberg; 2013, pp 1601-22.
5. Huang L-L, Xia HH-X, Zhu S-L. Ascitic Fluid Analysis in the Differential Diagnosis of Ascites: Focus on Cirrhotic Ascites. J Clin Transl Hepatol 2014;2:58-64.
6. Materka A. Texture analysis methodologies for magnetic resonance imaging. Dialogues Clin Neurosci 2004;6:243-50.
7. Varghese BA, Cen SY, Hwang DH, Duddalwar VA. Texture Analysis of Imaging: What Radiologists Need to Know. AJR Am J Roentgenol 2019;212:520-8.
8. Larroza A, Bodí V, Moratal D. Texture Analysis in Magnetic Resonance Imaging: Review and Considerations for Future Applications. In: Christakis Constantinides: Assessment of Cellular and Organ Function and Dysfunction using Direct and Derived MRI Methodologies. Intech Open 2016;1-21.
9. Strzelecki M, Szczypinski P, Materka A, Klepaczko A. A software tool for automatic classification and segmentation of 2D/3D medical images. Nuclear Instruments and Methods in Physics Research Section A: Accelerators, Spectrometers, Detectors Assoc Equip 2013;702:137-40.
10. Collewet G, Strzelecki M, Mariette F. Influence of MRI acquisition protocols and image intensity normalization methods on texture classification. Magn Resonance Imag 2004;22:81-91.
11. Karegowda A, Ma J, Manjunath AS. Cascading k-means clustering and k-nearest neighbor classifier for categorization of diabetic patients. Int J Engineer Advanced Technol 2012;1:147-51.
12. Skogen K, Schulz A, Dormagen JB, Ganeshan B, Helseth E, Server A. Diagnostic performance of texture analysis on MRI in grading cerebral gliomas. Eur J Radiol 2016;85:824-9.
13. Doi K. Computer-Aided Diagnosis in Medical Imaging: Historical Review, Current Status and Future Potential. Comput Med Imaging Graph 2007;31:198-211.
14. Tourassi GD. Journey toward computer-aided diagnosis: role of image texture analysis. Radiology 1999;213:317-20.
15. Tang X. Texture information in run-length matrices. Image Processing, IEEE Transactions 1998;7:1602-9.
16. Bjelakovic G, Tomislav T, Ivanka S et al. Biochemical, cytological and microbiological characteristics of the cirrhotic, malignant and "mixed" ascites. Arch Oncol 2001;9:95-101.
17. Baroud S, Schernthaner R, Mayerhoefer M, Wibmer A, Muin D, Ba'ssalamah A. Feasibility of Texture-based Classification of Different Types of Ascites at Contrast-enhanced Multidetector CT: Preliminary Results. RSNA Radiological Society of North America Annual Meeting 2011.